Embedding Information into Radar Emissions via Waveform Implementation

Shannon D. Blunt, Matthew R. Cook, and James Stiles
EECS Dept. / Radar Systems Lab
University of Kansas

***Abstract*— In this paper an approach for the joint design of multiple receive filters is described that enables the use of different waveforms during a radar CPI while minimizing the attendant Doppler coherency degradation due to range sidelobe clutter modulation. This capability allows for a set of unique radar waveforms to serve the dual purpose of acting as communication symbols while acceptable radar performance is maintained. The receive filter design approach is based upon the well-known Least-Squares (LS) mismatch filter formulation. The novel modification is the iterative adaptation of the desired response such that all the waveform/filter pair responses are driven to be identical.**

I. Introduction

Consider the diversity provided by changing the radar waveform on a pulse-to-pulse basis, *i.e.* pulse modulation diversity. One possible application of this capability arises if one views each of the possible waveforms as a communication symbol. Thus a desired receiver need only determine which of K possible waveforms was transmitted to obtain the $\log_2 K$ bits of embedded information. However, the real difficulty is in ensuring that the radar maintains adequate sensitivity.

For radar modalities where clutter cancellation is required it is important to maintain coherency over the set of M pulses within the coherent processing interval (CPI) or else the clutter will not be sufficiently cancelled and the residual clutter will degrade the sensitivity of the radar. Generally speaking, a radar will first pulse compress the received echoes using a filter that is nominally matched to the transmitted waveform (*e.g.* the Least-Squares mismatch filter trades off a small loss at the match point for lower range sidelobes [1]). For each range cell, Doppler processing is then applied across the set of M pulses. A clutter cancellation filter can be obtained by using training data over multiple range cells or by modeling the presumed clutter response. If different waveforms are employed over the CPI then the differences in the range sidelobe responses induces a loss in Doppler coherency, thus limiting the efficacy of clutter cancellation.

In this paper we consider how, for an arbitrary set of radar waveforms, the associated set of receive filters can be designed such that each of the waveform/filter pairs yields the same range sidelobe response. In other words, for $s_1(t), s_2(t), \cdots, s_M(t)$ the set of M waveforms in the CPI (drawn randomly from a set of K possible waveforms) and $h_1(t), h_2(t), \cdots, h_M(t)$ the set of associated receive filters, the constraint

$$s_1(t) * h_1(t) = s_2(t) * h_2(t) = \cdots = s_M(t) * h_M(t), \quad (1)$$

where $*$ is convolution, should be enforced. As such, assuming the absence of multiple-time-around clutter (hence applicable to relatively low PRF radars) the range-domain response of the clutter for each pulse will be the same thereby maintaining clutter cancellation performance. The inclusion of multiple-time-around clutter will be considered in future work.

It should be noted that, aside from the $K = 2$ case that will be discussed in Section III, the constraint in (1) cannot be exactly met unless one allows for infinite length filters. This fact can be shown by considering the frequency domain representation

$$S_1(\omega)H_1(\omega) = S_2(\omega)H_2(\omega) = \cdots = S_M(\omega)H_M(\omega) \quad (2)$$

which allows one to express the piece-wise relationship as

$$H_m(\omega) = \frac{S_1(\omega)H_1(\omega)}{S_m(\omega)} \quad (3)$$

where the presence of $S_m(\omega)$ in the denominator translates into $H_m(\omega)$ being an infinite impulse response (IIR) filter. As such, we shall employ an approach based on Least-Squares mismatch filtering that provides a good approximation to (1).

II. Radar Waveform Implementation

Due to the high fidelity requirements to perform clutter cancellation we shall use physically realizable radar waveforms as the basis for receive filter design. Chirp waveforms notwithstanding, the waveforms generated from binary codes are among the most commonly used today because they can be physically implemented in high power systems (*i.e.* they can be used with high power amplifiers) via implementation schemes such as derivative phase shift keying (DPSK) [2], minimum shift keying (MSK), and most recently continuous phase modulation (CPM) [3]. While the filter design approach developed herein is applicable to arbitrary codes and waveform implementations, for the purpose of brevity we shall restrict our attention to the commonly used DPSK implementation of binary codes.

For high power applications (*e.g.* long range surveillance) radar codes must be constant modulus so as to maximize the "energy on target". Nearly all codes are

This work was sponsored by the Air Force Office of Scientific Research and the Naval Research Laboratory – Radar Division.

designed with the implicit assumption that each code value is modulated onto a square-shaped chip thus leading to the idealistic radar waveform

$$s_{\text{ideal}}(t) = \sum_{n=0}^{N-1} e^{j\,x(n)} \left[u(t - n\tau) - u\left(t - (n+1)\tau\right) \right] \quad (4)$$

where τ is the chip interval, $u(t)$ is the unit step function, and $x(n)$ contains the sequence of N code phase values. As such, the phase shifts instantaneously if subsequent elements of the phase code $x(n)$ are different. This is, of course, impossible because infinite bandwidth would be necessary for an instantaneous transition. In contrast, consider the DPSK implementation of the code which is defined as

$$s_{\text{DPSK}}(t) = s_{\text{ideal}}\left(t - \tau/2\right) \left| \cos\left(\frac{\pi t}{\tau}\right) \right| - j\, s_{\text{ideal}}(t) \left| \sin\left(\frac{\pi t}{\tau}\right) \right| \quad (5)$$

where the radar code values are contained in $s_{\text{ideal}}(t)$ from (4). It is from the physically realizable waveform of (5) that we shall derive the subsequent LS mismatch filter. In so doing, the discretized waveform $\mathbf{s}_{\text{DPSK}}$ is a sampled version of $s_{\text{DPSK}}(t)$.

III. The Two Waveform Case

For the case of $K = 2$ possible waveforms, each pulse relays 1 bit of information such that a total of M bits are conveyed during an M pulse CPI. For this case the constraint from (1) simplifies to

$$s_1(t) * h_1(t) = s_2(t) * h_2(t). \quad (6)$$

This condition is straightforward to meet by setting

$$s_2(t) = s_1^*(-t), \quad (7)$$

for

$$h_1(t) = s_2(t) \text{ and } h_2(t) = s_1(t), \quad (8)$$

where $(\bullet)^*$ is complex conjugation. Thus each waveform is also the matched filter for the other.

At a communications receiver both filters can be applied to determine which of the two waveforms was transmitted. For example, for a randomly generated binary code of length $N = 50$ chips, it has been found that the unmatched filter having a correlation peak that is roughly 7 dB less than that for the matched filter it can be inferred that relatively low communication error performance can be achieved.

In practice the radar often employs a mismatch filter on receive to reduce the range sidelobes. However, the use of a mismatch filter violates the constraint of (1) as the conditions in (8) are no longer met. In Section V it will be shown how a modification to the Least-Squares mismatch filter design process provides the means to jointly design the set of filters for a set of arbitrary waveforms such that the resulting waveform/filter response is nearly identical over the K pairs.

IV. Least-Squares Mismatch Filtering

To achieve better range sidelobe performance for $K = 2$ waveforms or to increase the number of possible waveforms to $K > 2$, mismatch filtering is required. The following is a review of LS mismatch filter design [1].

We assume the use of a physically realizable waveform implemented using DPSK, MSK, or CPM to realize $s(t)$ which is subsequently sampled to obtain the vector $\mathbf{s}$ (multiple samples per chip are required to ensure that the mismatch filter adequately accounts for the continuum of receive echoes). From the discretized version of the radar waveform $\mathbf{s} = \begin{bmatrix} s_1 & s_2 & \cdots & s_{LN} \end{bmatrix}^T$, the $\tilde{N}L \times (\tilde{N}L - NL + 1)$ delay-shift matrix

$$\mathbf{A} = \begin{bmatrix} s_1 & 0 & \cdots & 0 \\ \vdots & s_1 & & \vdots \\ s_{LN} & \vdots & \ddots & 0 \\ 0 & s_{LN} & & s_1 \\ \vdots & & \ddots & \vdots \\ 0 & \cdots & 0 & s_{LN} \end{bmatrix} \quad (9)$$

is constructed where N is the number of chips in the code, L is the number of samples per chip taken from the continuous waveform $s(t)$, and $\tilde{N}L$ is the length (in samples) of the resulting mismatch filter with $\tilde{N}$ usually some multiple of N. Defining the linear model

$$\mathbf{A}\mathbf{h} = \mathbf{e}, \quad (10)$$

where $\mathbf{e} = \begin{bmatrix} 0 & \cdots & 0 & 1 & 0 & \cdots & 0 \end{bmatrix}^T$ is an elementary vector with the non-zero element corresponding to the match point (here denoted as the i^{th} element), Least-Squares estimation is used to estimate the filter $\mathbf{h}$ that most closely approximates the equality in (10) from a squared-error sense.

Before defining the LS filter estimate, first consider a well-known approach to trade range resolution for reduced range sidelobes for the LS mismatch filter formulation which is accomplished by replacing the elements in the rows of the matrix $\mathbf{A}$ surrounding the i^{th} row with zeroes. We shall zero out the $L/2$ rows above and the $L/2$ rows below the i^{th} row so that the sidelobes can be reduced to the point that nominal range resolution is achieved (*i.e.* the same as the matched filter). Denoting the resulting matrix with these rows zeroed as $\mathbf{B}$, the linear model of (10) can be restated as

$$\mathbf{B}\mathbf{h} = \mathbf{e}, \quad (11)$$

such that the nominal resolution mismatch filter can be computed as

$$\hat{\mathbf{h}}_{\text{LS}} = \left(\mathbf{B}^H\mathbf{B} + \delta\mathbf{I}\right)^{-1}\mathbf{B}^H\mathbf{e} \quad (12)$$

where $\delta\mathbf{I}$ is a diagonal loading term that is needed to prevent ill-conditioning since the waveform is over-sampled [1, 4] and the subscript 'LS' denotes the standard Least-Squares approach. It is the formulation in (11) and (12) that we will use to jointly optimize the set of filters for an arbitrary set of waveforms so as to satisfy the constraint in (1).

V. Joint Least-Squares Mismatch Filtering

Given a set of arbitrary physically realizable waveforms $s_1(t), s_2(t), \cdots, s_K(t)$ that could be employed for a given pulse (and thus can be viewed as the "constellation" of symbols from the communication perspective) denote their corresponding sampled versions as $\mathbf{s}_1, \mathbf{s}_2, \cdots, \mathbf{s}_K$, respectively. Following (12), a LS mismatch filter can be determined for the k^{th} waveform as

$$\hat{\mathbf{h}}_{\text{LS},k} = \left(\mathbf{B}_k^H \mathbf{B}_k + \delta\mathbf{I}\right)^{-1} \mathbf{B}_k^H \mathbf{e} \,. \tag{13}$$

As an example, Figure 1 illustrates the waveform/filter correlations for K = 4 randomly generated binary codes of length N = 50 where the waveforms are implemented using DPSK, sampled at a rate of L = 6 samples-per-chip, and the corresponding mismatch filters computed using (13) with $\tilde{N} = 5N$ and $\delta = 10$. While the resulting range sidelobe performance is good on an individual waveform/filter pair basis, the fact that the sidelobe structure varies over the pairs will hinder clutter cancellation as will be shown in Section VI.

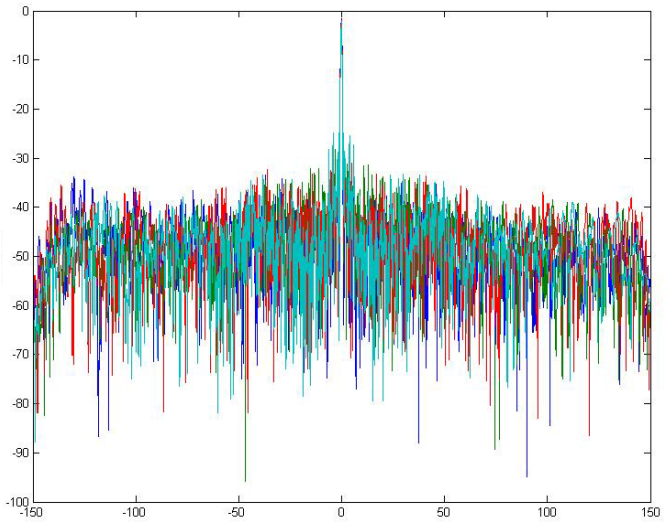

Figure 1. Waveform/filter correlations using traditional LS mismatch filters

To incorporate the constraint of (1), consider the result of substituting the filter from (13) back into the original linear model of (11) for the k^{th} waveform which yields

$$\mathbf{B}_k \hat{\mathbf{h}}_k = \mathbf{r}_k \,, \tag{14}$$

where $\mathbf{r}_k$ is the actual result from the matrix multiplication $\mathbf{B}_k \hat{\mathbf{h}}_k$. Note that $\mathbf{r}_k$ is similar to, but not exactly the same as, the associated waveform/filter correlation because the zeroed rows in $\mathbf{B}_k$ set the $L/2$ elements before and after the match point in $\mathbf{r}_k$ to zero as well. Using $\mathbf{r}_k$ for $k = 1, 2, \cdots, K$ we wish to devise a new desired response (to replace $\mathbf{e}$ in (12)) so as to drive the set of K waveform/filter pairs closer to meeting (1). The goal is to find a range sidelobe structure that lies within the space of feasible solutions for all waveform/filter pairs. There are numerous possible ways in which the $\mathbf{r}_k$ vectors could conceivably be combined including computing the mean across the vectors, a simple minimization of sidelobes across the vectors, piece-wise error minimization, etc. Here we shall consider the simple mean operation defined as

$$\bar{\mathbf{r}} = \sum_{k=1}^{K} \mathbf{r}_k \,. \tag{15}$$

Note that because the LS mismatch filter generally results in some small amount of loss at the match point (the i^{th} element of $\mathbf{e}$ that is '1'), this element in $\bar{\mathbf{r}}$ should be reset to '1' to avoid the accumulation of mismatch losses that could otherwise occur through iterative application of the design procedure to follow.

Given $\bar{\mathbf{r}}$ from (15) computed after applying (13) and (14) for a set of arbitrary waveforms, the set of K filters can be recomputed with the new desired response as

$$\hat{\mathbf{h}}_{\text{JLS},k} = \left(\mathbf{B}_k^H \mathbf{B}_k + \delta\mathbf{I}\right)^{-1} \mathbf{B}_k^H \bar{\mathbf{r}} \tag{16}$$

where the subscript 'JLS' denotes Joint Least-Squares. By iteratively repeating (14)-(16), resetting the match point value in the updated $\bar{\mathbf{r}}$ each iteration, it has been found that the resulting set of waveform/filter responses tend toward one another such that (1) is approximately achieved. For example, using the same waveforms from Figure 1, the application of this process for 50 iterations yields a new set of 4 jointly optimized LS mismatch filters that provide the waveform/filter responses shown in Figure 2. It is obvious that, while not exact, these responses very closely match one another.

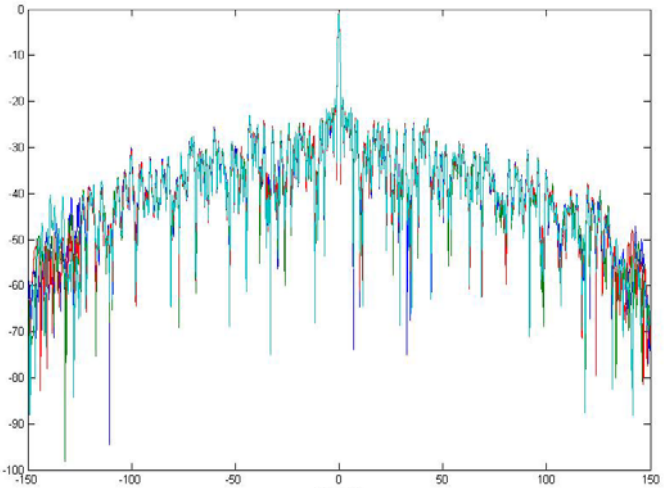

Figure 2. Waveform/filter correlations using jointly optimized LS mismatch filters

It can be observed by comparing Figures 1 and 2 that the range sidelobes in the latter are higher than in the former. This increase in range sidelobes occurs because the set of filters are driven to determine the response that is feasible for all waveform/filter pairs which, due to finite degrees-of-freedom, is unlikely to also achieve a minimum sidelobe solution equivalent to that of the original LS filters. For this reason it is expected that the range sidelobe levels would likewise increase as the number of different waveforms K increases. However, as will be shown in Section VI, the trade-off in the range sidelobe level is compensated by closely approximating the constraint in (1) which subsequently enables superior clutter cancellation performance. It should likewise be noted that the underlying binary codes were in no way optimized for good radar performance and it is possible that joint determination of optimal codes may likewise provide a benefit for the design of these jointly optimized filters.

Given that one of the goals of the filter design process here, besides the obvious one of yielding a viable response with low range sidelobes, is to achieve a close approximation to the constraint of (1), we can define a metric to assess the improvement of the set of jointly optimized filters with respect to the original filters. Denoting the vectors $\mathbf{g}_{\mathrm{LS},k} = \mathbf{s}_k * \hat{\mathbf{h}}_{\mathrm{LS},k}$ and $\mathbf{g}_{\mathrm{JLS},k} = \mathbf{s}_k * \hat{\mathbf{h}}_{\mathrm{JLS},k}$ as the k^{th} waveform/filter responses for the Least-Squares and Joint Least-Squares filters, respectively, define the matrices $\Delta\mathbf{G}_{\mathrm{LS}}$ and $\Delta\mathbf{G}_{\mathrm{JLS}}$ where the i, j element of each is, respectively, $\left\|\mathbf{g}_{\mathrm{LS},i} - \mathbf{g}_{\mathrm{LS},j}\right\|$ and $\left\|\mathbf{g}_{\mathrm{JLS},i} - \mathbf{g}_{\mathrm{JLS},j}\right\|$. Thus, the metric

$$\eta = \frac{\left\|\Delta\mathbf{G}_{\mathrm{JLS}}\right\|_F^2}{\left\|\Delta\mathbf{G}_{\mathrm{LS}}\right\|_F^2}, \tag{17}$$

where $\left\|\bullet\right\|_F^2$ is the squared Frobenius norm, provides a measure of the reduction in total piece-wise squared error across the set of waveform/filter pairs. For the sets of filters shown in Figures 1 and 2, the value of this metric was found to be $\eta = -8.7$ dB. While this metric does not necessarily provide a direct measure of overall performance improvement (again, it does not determine the impact of increased range sidelobes), it does enable the comparison of filter sets in terms of their ability to maintain clutter cancellation performance when pulse modulation diversity is employed.

VI. Clutter Cancellation Performance

To assess the benefit of jointly optimizing the set of K mismatch filters to maintain clutter cancellation capability when pulse-to-pulse waveform modulation is employed we consider a simulated scenario where a single target (15 dB SNR after coherent integration due to pulse compression and Doppler processing) is masked by clutter at a level of 50 dB CNR after coherent integration. The CPI consists of 20 pulses where the waveform for each pulse is randomly selected from the set of K = 4 waveforms of DPSK-implemented binary codes of length N = 50 shown previously. The clutter is modeled as three superimposed white Gaussian processes where one is stationary in slow-time and the other two provide a small amount of clutter Doppler spread to approximate the effects of internal clutter motion. The clutter range interval contains 500 range cells with the target in the center such that, with the receive filters extending over 250 range cells, no unrealistic windowing effects are experienced. Only the center 100 range cells are shown in the results to provide easier visualization.

Simple clutter cancellation is employed using a narrow notch (0 Doppler bin) and a wide notch (the 0 Doppler bin as well as ±1 Doppler bins on either side) to better suppress Doppler-spread clutter. The clutter cancellation filters are based on a straightforward diagonally-loaded projection matrix using the corresponding steering vector(s) to be suppressed. All clutter-suppressed range-Doppler images are scaled to show the highest 40 dB interval of the residual output for each.

Figures 3 and 4 depict the range-Doppler images after applying the narrow-notch and wide-notch clutter filters, respectively, for the case where standard LS pulse compression filters are employed. It is observed that the wide-notch clutter filter (Fig. 3) provides some improvement on clutter suppression with respect to the narrow-notch filter (Fig. 4) as the latter fails to suppress some of the Doppler-spread clutter. However, for both cases the target (indicated by the black circle), while visible, is unlikely to be detected when using CFAR detection due to the presence of numerous range-Doppler sidelobes throughout the image that arise from inadequate clutter cancellation as a result of sidelobe clutter modulation effects.

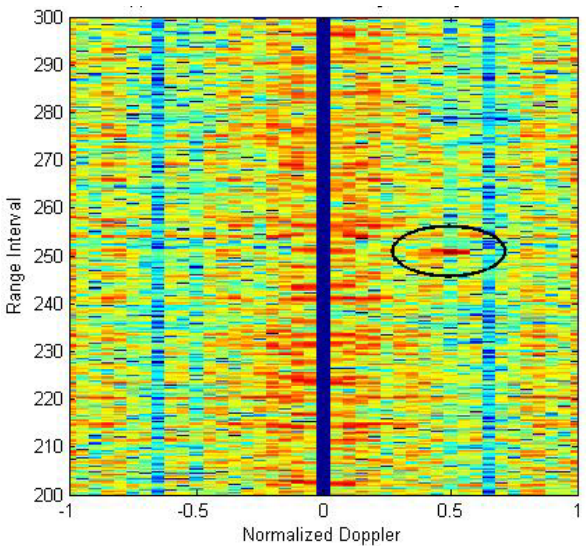

Figure 3. Range-Doppler image after narrow-notch clutter cancellation using traditional LS mismatch filters

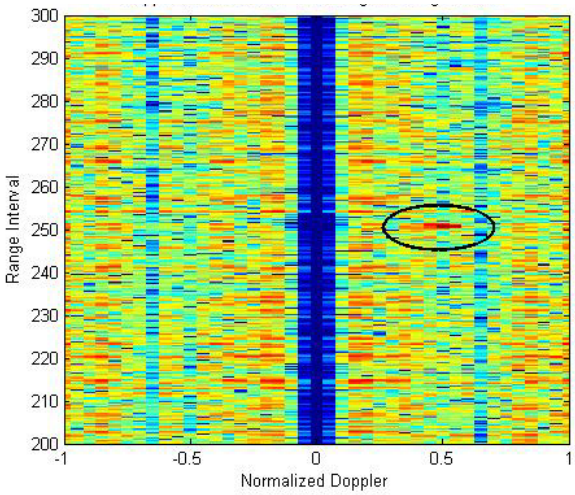

Figure 4. Range-Doppler image after wide-notch clutter cancellation using traditional LS mismatch filters

In contrast, Figures 5 and 6 illustrate the clutter cancellation performance when the pulse compression mismatch filters are jointly optimized to provide nearly identical responses. For the narrow-notch case in Figure 5 the target is clearly visible and may possibly be detected despite the residual Doppler-spread clutter. For the wide-notch case in Figure 6 the residual clutter is suppressed almost completely such that the target is the only remaining large artifact. In this latter case it was found that the peak value of the target was at least 12 dB above all the other range-Doppler cells in the image.

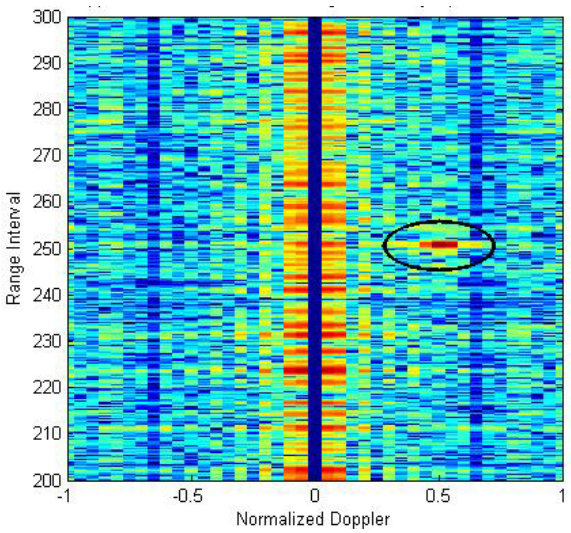

Figure 5. Range-Doppler image after narrow-notch clutter cancellation using joint LS mismatch filters

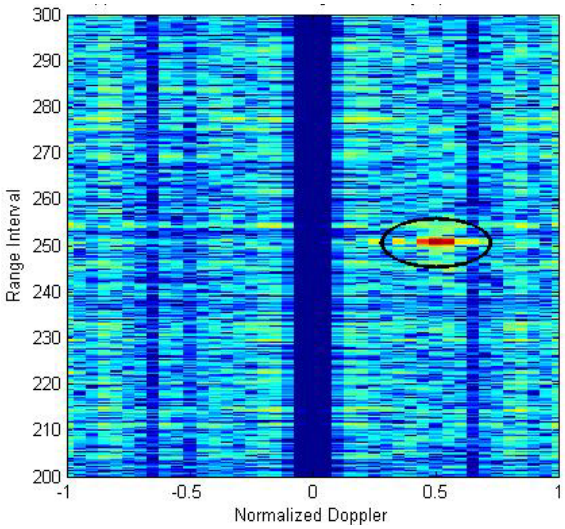

Figure 6. Range-Doppler image after wide-notch clutter cancellation using joint LS mismatch filters

VII. Conclusions

A modified form of Least-Squares mismatch filter estimation has been developed that allows for the trade-off between range sidelobe levels and the coherency of the range sidelobes for an arbitrary set of illuminating waveforms so as to maintain sufficient clutter cancellation performance. For relatively low PRF radars where multiple-time-around clutter can be neglected, this new set of receive filters facilitates the use of pulse modulation diversity. One possible application of this scheme is to allow the radar waveforms to serve the dual purpose of being communication symbols so that the radar can additionally transmit information as well as perform its primary function of sensing. Future problems to be explored include the joint optimization of the set of radar waveforms, the accommodation of multiple-time-around clutter, alternative optimization metrics within the filter design process, holistic performance metrics that assess both range sidelobe levels and Doppler coherency, and the performance assessment of the communication system for which the embedded information is intended.

VIII. References

[1] T. Felhauer, "Digital signal processing for optimum wideband channel estimation in the presence of noise," *IEE-Proc.-F*, vol. 140, no. 3, pp. 179-186, June 1993.

[2] H. Faust, B. Connolly, T.M. Firestone, R.C. Chen, B.H. Cantrell, and E.L. Mokole, "A spectrally clean transmitting system for solid state phased-array radars," *IEEE Radar Conf.*, 26-29 April 2004, pp. 140 – 144.

[3] S. Blunt, M. Cook, E. Perrins, and J. de Graaf, "CPM-based radar waveforms for efficiently bandlimiting a transmitted spectrum," *IEEE Radar Conf.*, Pasadena, CA, 4-8 May 2009.

[4] S.D. Blunt, K. Gerlach, and T. Higgins, "Aspects of Radar Range Super-Resolution," *IEEE Radar Conference*, Waltham, MA, pp. 683-687, 17-20 April 2007.